NIH Public Access
Author Manuscript
Sens Actuators B Chem. Author manuscript; available in PMC 2011 April 8.

Published in final edited form as:
Sens Actuators B Chem. 2010 April 8; 146(1-8): 297–306. doi:10.1016/j.snb.2010.02.009.

Multi-wavelength Spatial LED illumination based detector for *in vitro* detection of Botulinum Neurotoxin A Activity

Steven Sun[1,2], **Jesse Francis**[2], **Kim E. Sapsford**[1], **Yordan Kostov**[2], and **Avraham Rasooly**[1,3]

[1]Division of Biology, Office of Science and Engineering Laboratories, FDA, Silver Spring, MD 20993, USA.

[2]University of Maryland Baltimore County (UMBC), Baltimore, MD 21227, USA.

[3]National Cancer Institute, Rockville, MD 20892

Abstract

A portable and rapid detection system for the activity analysis of Botulinum Neurotoxins (BoNT) is needed for food safety and bio-security applications. To improve BoNT activity detection, a previously designed portable charge-coupled device (CCD) based detector was modified and equipped with a higher intensity more versatile multi-wavelength spatial light-emitting diode (LED) illumination, a faster CCD detector and the capability to simultaneously detect 30 samples. A FITC/DABCYL Förster Resonance Energy Transfer (FRET)-labeled peptide substrate (SNAP-25), with BoNT-A target cleavage site sequence was used to measure BoNT-A light chain (LcA) activity through the FITC fluorescence increase that occurs upon peptide substrate cleavage. For fluorescence excitation, a multi-wavelength spatial LED illuminator was used and compared to our previous electroluminescent (EL) strips. The LED illuminator was equipped with blue, green, red and white LEDs, covering a spectrum of 450-680 nm (red 610-650 nm, green 492-550 nm, blue 450-495 nm, and white LED 440-680 nm). In terms of light intensity, the blue LED was found to be ~80 fold higher than the previously used blue EL strips. When measuring the activity of LcA the CCD detector limit of detection (LOD) was found to be 0.08 nM LcA for both the blue LED (2 s exposure) and the blue EL (which require ≥60 s exposure) while the limits of quantitation (LOQ) is about 1 nM. The LOD for white LED was higher at 1.4 nM while the white EL was not used for the assay due to a high variable background. Unlike the weaker intensity EL illumination the high intensity LED illumination enabled shorter exposure times and allowed multi-wavelength illumination without the need to physically change the excitation strip, thus making spectrum excitation of multiple fluorophores possible increasing the versatility of the detector platform for a variety of optical detection assays.

Keywords

LED; Electroluminescent excitation; CCD; fluorescence; Förster resonance energy transfer (FRET); Botulinum neurotoxin A; Biodetection

Publisher's Disclaimer: This is a PDF file of an unedited manuscript that has been accepted for publication. As a service to our customers we are providing this early version of the manuscript. The manuscript will undergo copyediting, typesetting, and review of the resulting proof before it is published in its final citable form. Please note that during the production process errors may be discovered which could affect the content, and all legal disclaimers that apply to the journal pertain.

NIH-PA Author Manuscript
NIH-PA Author Manuscript
NIH-PA Author Manuscript

NIH-PA Author Manuscript
NIH-PA Author Manuscript
NIH-PA Author Manuscript

1. Introduction

Of the seven serotypes (A–G) of Botulinum Neurotoxins (BoNT) produced and secreted by *Clostridium botulinum*, four of them (A, B, E, and F) are normally associated with human illness and are among the most deadliest known toxins. BoNT neurotoxicity results from BoNT light chain subunit cleavage of the soluble *N*-ethyl maleimide-sensitive fusion protein attachment protein receptors (SNAREs) of the presynaptic vesicles required for neurotransmitter release. Early detection and typing of these toxins is critical for food safety, bio-security and clinical diagnostic applications where it is essential for providing appropriate and timely medical treatment by enabling the selection of effective antitoxins. Detection of BoNT for such applications (e.g. in the field without a laboratory) may require a portable and rapid detection system capable of measuring both the presence and activity of the toxin.

In general, three types of detection approaches for BoNT measurement have been developed; (1) immunological assays which detect the presence of the toxin (active or not), (2) *in vivo* bioassays for toxin activity analysis (such as the mouse bioassay) and (3) the detection of toxin activity by *in vitro* peptide cleavage assays. Several different immunoassays have been developed for BoNT detection including enzyme-linked immunosorbent assays (ELISA) [1-6], lateral flow immunoassays [7,8], immunomagnetic beads [9,10] and immunoaffinity column [11,12]. More complex immunological technologies have been developed for BoNT detection including; a portable evanescent wave immunosensor combined with a fluidics system [13-15], a magnetic bead based ELISA with electrochemiluminescent detection [16] which combines automated flow-through capillary gel electrophoresis with laser-induced fluorescence detection, an optical silicon chip assay which detects physical changes in the thickness of a functionalized molecular thin film resulting from specific immunobinding events [17] and a two-step immunometric assay detected using a Acetylcholinesterase (AChE) assay [18]. Recently, a simple monoclonal antibody-based lateral flow assay for detection of BoNT-A enabled the detection of 50 ng/mL in less than 10 min, with the assay sensitivity increased to 1 ng/mL by silver enhancement [19]. While some of these immunoassays have similar sensitivities to the gold standard mouse bioassay [20-22] and are capable of rapid toxin analysis, they do not provide information about the activity state of the toxin.

The traditional *in vivo* mouse bioassay measures the effects of the toxins on a mammalian organism (e.g. signs of botulism in mice) and is very sensitive, detecting as little as 0.03 ng of botulinum toxin (1 ng = 30 mouse 50% lethal doses) within 6-96 hours [23,24]. However, the mouse bioassay is slow and the use of live animals is not practical for rapid, field-deployable applications. BoNT activity can be detected by assaying the cleavage function of the toxin using specific peptide target substrates. For example, Synaptosomal-associated protein 25 (SNAP-25) peptide is specific to BoNT-A [3,25-32]. Synaptosomal-associated protein 25 (SNAP-25) is a membrane bound protein involved in membrane fusion which functions as part of the neuromuscular junction. BoNT- A light chain (LC-A) is an endopeptidase which cleaves SNAP-25 and thus prevents vesicles from anchoring to the membrane to release the neurotransmitter acetylcholine.

A number of researchers have used this approach and some of the technical issues concerning these protease-based activity assays, including matrix inhibition and non-specific cleavage signals, were recently addressed [33-35].

BoNT cleavage activity have been detected using three types of methods; 1) applying specific antibodies that recognize the proteolytically generated cleavage product epitope for BoNT [20,23], 2) changes in mass of the cleaved peptide detected by mass spectrometry, cantilevers or surface plasmon resonance (SPR) [3,12,22,28,30,32], and 3) using short peptide sequences fluorescently labeled with Förster Resonance Energy Transfer (FRET) pairs in which toxin

NIH-PA Author Manuscript

NIH-PA Author Manuscript

NIH-PA Author Manuscript

mediated cleavage results in a change in the fluorescent signal. Immunological detection, for example, was demonstrated for BoNTC1 [36] and BoNT-B activity [37], with the target for immunological detection being an octapeptide epitope sequence that is normally buried within the native substrates alpha-helical structure but becomes exposed following cleavage by toxin types A or E [38]. Most of these cleavage-based detection methods require specialized equipment (MS, SPR, cantilever, etc), which can limit broad utilization of the technology. Therefore the most popular detection of BoNT cleavage activity is based on FRET-labeled peptide substrates that detect the cleavage of the toxins target peptides substrate though changes in fluorescence that can be measured via a variety of fluorescent sensors [32].

Various aspects of FRET based assay for BoNT activity have been studied, the assay conditions were optimized [39,40] and the target peptides have also been optimized, including shorting the linker peptide between the two fluorophores and doubling the number of the FRET acceptors especially in peptide sequences containing two substrate specific sites [41]. Recombinant fluorescent substrate with cleavage sites for BoNT serotypes A, B, and E in high-throughput screening were developed [42]. Other approaches include; an immunomagnetic bead-based pre-concentration step, utilizing antibodies directed against the 100-kDa heavy chain subunit to concentrate the toxin prior to detection with the FRET cleavage assay, thus enabling similar sensitivity to the mouse bioassay [34,35,43]. In this fluidics system there is a large “reservoir” containing the toxin sample with the peptide-beads and a smaller “reservoir.” Both are connected with a microchannel. After incubation, during which the toxin cleaves the peptide, the system is placed in a non-humidified environment, generating evaporative flow from the large reservoir to the small detection port and thus concentrating the beads.

Several microfluidic devices have been developed for fluorescent-based cleavage assays including bead-based microfluidic platform utilizing peptide immobilized on beads, which when cleaved by the toxin releases fluorescent fragments into solution that can be concentrated and detected using microscopy [44] and molded silicone microdevices with integral valves, pumps, and reagent reservoirs combined with electrical and pneumatic control [45]. However, for both microfluidic platforms described fluorescence detection was accomplished by fluorescence microscopy, limiting the field application of the device.

Clearly, while extensive research has been conducted to improve the cleavage assay most use either standard plate readers or fluorescence microscopy and little work has been done to improve the fluorescent detectors needed to run such assays under field deployable/limited laboratory availability type applications. Developing portable devices which enable the assay performance outside the laboratory, require an easy-to-use multi-sample format that is both sensitive and portable. One of the critical elements for such optical based detectors is the light source used for fluorescence excitation. Although a broad array of illumination sources are available to researchers (e.g. lasers, LED, tungsten lamps etc), almost all are spot illuminators with narrow spatial field of illumination. Therefore, excitation of a relatively large surface area needed for multiple sample analysis requires either scanning (moving the light source or moving the surface to be scanned), the use of a panel of excitation sources, or incorporation of a number of optical components such as waveguides, line generators, mirrors and lenses [13-15]. Such optical components complicate platform design, manufacturing, maintenance, and add to the overall cost. In our previous work [46] we used phosphor based electroluminescent (EL) semiconductor strips for spatial illumination over a relatively large surface area. The resulting EL-based charged-coupled device (CCD) portable detector platform was used for measurement of the BoNT-A FRET cleavage activity assay, and although simple, sensitive and effective, the EL low light intensity required long CCD exposure times (e.g. 30 s up to 2 min.). Also, while the EL strips are available in different wavelengths, each wavelength requires a different EL, requiring manual switching by the user when changing excitation wavelength complicating the overall design of an optical detector with multi-wavelength

NIH-PA Author Manuscript

NIH-PA Author Manuscript

NIH-PA Author Manuscript

capabilities. LEDs are, likewise, available with many wavelengths and provide higher light intensity than the EL strips. However, LEDs have narrow spatial field of illumination and so to overcome this limitation, the use of multiple LEDs combined with a diffuser was used to enable simple spatial illumination. The LED-CCD detector described in this study was designed with the aim of producing a portable, simple, and inexpensive modular-based optical detection system with the capability of multi-wavelength illumination for the analysis of various flurophores in a relatively small and compact manner, capable of measuring multiple samples simultaneously. The resulting platform could be used to measure fluorescence from a number of standard formats such as solution fluorometers, slide microarrays, PCR and ELISA assays.

2. Material and Methods

2.1 Materials and Reagents

All chemicals were of reagent grade and used as received from the manufacturer. Bovine Serum Albumin (BSA), zinc chloride (ZnCl), and *N*-[2-hydroxyethyl] piperazine-*N*'[2-ethane sulfonic acid] (HEPES) were obtained from Sigma-Aldrich (St. Louis, MO). The SNAP-25 peptide substrate, internally labeled with the FRET pair fluoresceinthiocarbamoyl (FITC) and 4-(dimethylaminoazo)benzene-4-carboxylic acid (DABCYL), was purchased from List Biological Laboratories (FITC/DABCYL-SNAP-25; Campbell, CA). Also obtained from List Biological Laboratories was the positive control FITC-labeled SNAP-25 (FITC-SNAP-25; not labeled with acceptor DABCYL) and the recombinant light chain of BoNT-A (LcA). The 30-well sample chips, used to hold the samples for analysis, were prepared using 1/8 inch black Poly(methyl methacrylate) (PMMA) also known as acrylic (Total Plastics, Harrisburg, PA) and a transparent plastic Polyethylene terephthalate polycarbonate (PC) (Piedimont Plastic Inc, Beltsville, MD) was used as base and top for the 30-well chip.

2.2 FRET Fluorescence Detection

For FRET excitation, an LED illumination box containing red, green, blue, and white LEDs was custom built by Luminousfilm (Shreveport, Louisiana, www.luminousfilm.com/led.htm). The EL strips [47] consist of either a Royal Blue EL strip or Bright White EL strip cut to 2.5 × 5 cm (Being Seen Technologies, Bridgewater, MA). The EL strips required 110 AC volts supplied by an inverter which converts the 12 volts DC input into 110 volts AC output (Being Seen Technologies, Bridgewater, MA). The detection system consisted of a blue excitation filter HQ480/20x (Chroma Technology Corp, Rockingham, VT), a green emission filter D535/40m (Chroma Technology Corp Rockingham, VT), and a cooled astronomy Sony ICX-429ALL 752×582 pixel CCD camera connected to a Windows XP PC via a USB2 port and controlled using SXVF-M7 Capture software (CCD camera and software: Adirondack Video Astronomy, Hudson Falls, NY). The CCD camera was equipped with a Tamron manual zoom CCTV 4-12 mm, f1.2 (Spytown, Utopia, NY), and all the system components were enclosed custom in-house built black acrylic box. The CCD image intensities were analyzed using ImageJ software, developed and distributed freely by NIH (http://rsb.info.nih.gov/ij/download.html), and the data generated is then imported into Microsoft Excel (Microsoft, Redmond, WA) for further manipulation.

2.3 Fabrication of the 30-Well Sample Chips

The 30-well sample chips used in this study were designed in CorelDraw11 (Corel Corp. Ontario, Canada) and micro-machined in 1/8 inch black acrylic using a computer controlled laser cutter Epilog Legend CO2 65W cutter (Epilog, Golden, CO). Before cutting, both sides of the acrylic sheet was coated with 3M 9770 adhesive transfer double sided tape (Piedmont Plastics, Beltsville, MD). For sealing the base and top of the 30-well acrylic sample chips, PC was first attached to the double sided tape, following cutting using the laser cutter, the PC was

NIH-PA Author Manuscript

NIH-PA Author Manuscript

NIH-PA Author Manuscript

then attached to the bottom on the 30-well acrylic sample chip by removing the protective cover on the double sided tape and firmly pressing the material into place. The reaction solution was added to the sample wells and the well tops carefully sealed (so as not to introduce air bubbles) with a PC top if required.

2.4 Optimization Studies using Unquenched FITC-SNAP-25

Initial investigations characterizing the different illumination sources were carried out using unquenched FITC-SNAP-25. Typically, a range of FITC-SNAP-25 concentrations were first prepared between 0.019 nM-5 nM in 20 mM HEPES + 0.3 mM ZnCl + 1 mg/ml BSA and 1.25 mM DTT (HEPES/Zn/BSA/DTT buffer), in MicroAmp tubes (PE Biosystems, Foster City, CA). A negative control (no FITC-SNAP-25) was included in each assay. The samples in the MicroAmp tubes were then loaded to the 30-well sample chips (12 μl/well) for measurement with the CCD detector coupled to the various LED and EL illumination sources.

2.5 FRET Cleavage Assay for LcA Activity Detection

The FITC/DABCYL-SNAP-25 FRET-based assay used in this study for the detection of light chain (LcA) was performed following the manufacturer's instructions. Typically, a range of LcA concentrations were first prepared between 0.08 nM-20 nM in 20 mM HEPES + 0.3 mM ZnCl + 1 mg/ml BSA and 1.25 mM DTT (HEPES/Zn/BSA/DTT buffer) in MicroAmp tubes. A negative control (no LcA) was included in each assay. The FITC/DABCYL-SNAP-25 was then added to each MicroAmp tube, to a final concentration of 5 μM per tube. These samples were then incubated, at 37 °C for 2 h, in the MicroAmp tubes. After incubation the samples in the MicroAmp tubes were transferred to the 30-well sample chips (12 μl/well) for measurement with the CCD detector coupled to the various LED and EL illumination sources.

3. Results and Discussion

3.1 Multi- wavelength LED illumination based fluorescence detector (LED-CCD)

In our assay (see figure S1) we use a short synthetic peptide with the sequence of the cleavage site of SNAP-25 that mimics the actual BoNT cleavage substrate. The peptide is labeled with a FRET pair, made up of a donor chromophore that, when excited, can transfer energy to an acceptor chromophore located in close proximity thereby “quenching” the fluorescence. When the toxin cleaves the peptide, it separates the donor chromophore from the acceptor, eliminating the quenching and resulting in full fluorescence of the donor chromophore as measured by CCD.

The basic configuration of the LED-CCD detector platform is shown schematically in Figure 1A along with an actual photograph of the detector Figure 1B. The system consists of three main elements (described in more detail below), the CCD detector module, the assay chip module and the illumination/excitation module, all contained within a black acrylic box.

LED Illumination module—The LED illumination module used in this study comprises a custom built multi-wavelength LED illumination box (Figure 1C). Two different types of LED were used: white LEDs and RGB LED (an RGB LED that can generate all three wavelengths). The multi-wavelength LED illumination box can illuminate with red (R), green (G), blue (B) or white (W) spectra (Figure 1D where each spectra is labeled with a letter under its peak white-W, blue-B, green-G and red-R). Although only illumination in the blue range is needed for the FITC excitation used in this study, the multi-wavelength illumination is capable of exciting multiple fluorophores making this a versatile detector for a variety of optical fluorescent assays. The LED illuminator contains four RGB LED strips and four daylight LED strips, both 18 LEDs per foot. Each LED color is controlled individually with a switch in the front panel (see Figure 1C). The top of the box consists of a diffusion panel (milky white plastic panel), which

NIH-PA Author Manuscript

NIH-PA Author Manuscript

NIH-PA Author Manuscript

assures uniformity of the light and hence even illumination of the sample chip. The dimensions of the diffusion panel are 8.5×5.5 cm. The blue excitation filter was taped, using black tape, on top of the diffusion panel and the assay chip module was then placed on top. For comparison, white and blue EL strips were also used as excitation sources. These were typically placed on top of the LED illuminator box (which was switched off) and the blue excitation filter then placed above the EL strip before the assay chip module was attached.

Assay module—The LED-CCD detector is compatible with a broad array of assay formats and various microfluidics. In this work, 30-well assay chips (Figure 1E), arranged in an array of 6×5 wells, were used. The 30-well sample chip was prepared using a laser cutter to cut black acrylic, which was chosen in order to minimize light scattering and cross talk between wells. The assay chip is simply loaded with the sample and placed above the illumination module prior to measurement. The maximum number of wells that were used in such a system is 96.

CCD detector—We used a cooled SXVF-M7 astronomy-CCD camera, where cooling reduces the thermal noise generated by the CCD and thus improves the sensitivity by reducing the background signal. The camera is equipped with a Sony ICX-429ALL 752×582 pixel CCD chip with a 16 Bit analog-to-digital converter enabling a dynamic range of 65,536 levels of grayscale. The SXVF-M7 camera was equipped with a USB2 port, enabling faster data transmission, and can be controlled with Labview software, allowing simple system automation. The fixed angle Pentax 12mm lens used in previous LcA work [47] was replaced with a Tamron manual zoom CCTV 4-12 mm, f1.2 lens. The 4 mm focal length of the lens permits wide angle imaging suitable for 96-well sample analysis [48] (e.g. 50×35 mm surface) from a short distance (9 cm). For the BoNT-A activity assay described in this work, a green pass band emission filter was mounted on the end of the lens.

Power considerations—For a portable device, the power requirements are an important element of the device design. The device was designed to be battery operated using 12V DC (supplied by either a power supply or battery such as commonly used for car batteries and many other portable devices) to run both the illumination source and the CCD.

3.2. Light characteristics of the multi-wavelength LED illuminator

Unlike the monochromatic light emitted from lasers or the limited spectrum light emitted from single LED and EL based illumination, the multi-wavelength LED illumination box provides illumination in the blue, green, red, and white ranges, covering a spectrum of 450-650 nm (red 610-650 nm, green 492-550 nm and blue 450-495 nm). The only region of the spectrum not represented by the RBG LEDs strip is the range between 550 nm and 610 nm. However, this region is provided by the white LED (Figure 2A), which gives broad band illumination (440-680 nm with lower intensity in the range 472-510 nm). The box allows for illumination in narrower spectra by using only one of the R,B,G, or white LEDs or combinations of them. Within each LED spectrum, interchangeable filters can be used to narrow the excitation band.

The BoNT-A FRET-based activity assay used here is based on FITC measurement, which requires an excitation wavelength of 494 nm therefore, we analyzed the white and the blue LED spectrum in more detail. As discussed above, the white LED emits light in a broad spectrum (440-680 nm with lower intensity in the range 472-510 nm) and the blue LED emits in the range 450-495 nm with a peak at 470 nm. A blue pass filter HQ480/20x with a range of 463-490 nm was used for FITC excitation. Since the excitation source is directly in line with the CCD camera in our device configuration, the excitation and emission filters are crucial for blocking any excitation light reaching the detector, while still allowing the fluorescence emission through. A comparison of the white and blue LEDs and ELs spectra, with and without the blue band pass excitation filter, is shown in Figure 2 A-D, and was measured using a SPA-

NIH-PA Author Manuscript

NIH-PA Author Manuscript

NIH-PA Author Manuscript

RP Reflectance Probe spectrometer. In figure 2, each spectrum is labeled with a number, I for the spectrum without a filter and II for the spectrum with a filter. An arrow points to the peak of the spectrum with a filter, the blue filter seems to decrease the intensity significantly in the blue range only for white LED illumination (figure 2A –II).

When comparing the blue (Figure 2A) and white (Figure 2B) LEDs it is apparent that the intensity of the blue LED is generally less than that of the white LED in the blue range. With an exposure time for the LED illumination of 100 ms, the intensity for white LED with this filter (at 475 nm) is 65 units above background (Figure 2A) and for the blue LED intensity is 50 units (Figure 2B). Longer exposure times were typically required to obtain spectra from the EL strips. Figure 2C and 2D show spectra using 5 s exposure times for the white and blue ELs respectively. The intensity for the white EL was 300 units (Figure 2C) and for the blue EL was 900 units (Figure 2D). Taking into account the different exposure times, the data suggests that at 475 nm the intensity of the white LED was ~11 fold higher than the white EL and the blue LED ~3 fold more intense than the blue EL. Light intensity and uniformity was measured directly using the cooled CCD detector and analyzed using ImageJ 3D analysis. Results demonstrated that the LED diffusion panel provides highly uniform illumination (Supporting Information, Figure S2).

Light intensity—One limitation of EL as a light source for fluorescence detection is its relative low light intensity (Figure 2C and 2D) which requires longer exposure. The true measure of the excitation's effectiveness is the actual fluorescence of the excited dye. To study the effectiveness of the various illuminators for FITC fluorescent detection, we measured the excitation of 5 nM unquenched SNAP-25 peptide (labeled only with FITC) detected with a cooled CCD camera equipped with a blue emission filter and green excitation filter for monitoring for emission at 523 nm. As shown in Figure 2E, the log signal measured is linearly correlated with the log time of exposure for the white (white circles), blue LEDs (black circles), and for the blue electroluminescence panels (black triangles) with an r^2>0.99 for all three illuminators. The regression lines (Figure 2E) are: white LED Y=4.34+0.82X; Blue LED Y=3.76+0.82X; and blue EL Y=2.37+0.76X. These data suggest that the FITC fluorescence signal from white LED illumination is ~3 fold higher than from illumination with blue LED, corresponding to the higher intensity of the white LED as shown in Figure 2. The fluorescence signal from illumination with the blue LED is ~80 fold higher than the signal from illumination with the blue EL, which suggests exposure time from EL must be far longer than to LED to achieve the same signal.

3.3 LED-CCD and EL-CCD fluorescence assay analysis using unquenched FITC-SNAP-25 peptide

To evaluate LED-CCD detection capabilities as compared to the EL-CCD and to optimize assay detection, we first measured emission of the unquenched SNAP-25 peptide at nine concentrations ranging from 0.019 nM - 5 nM, plus a blank control. For these tests, three 30-well chips were used with three replicas of each concentration in each chip. The layout of the 30 well chip is shown in figure S3.

FITC-SNAP-25 peptide was excited with white and blue LEDs as well as the white and blue EL strips. Various exposure times for each of the illumination modes were used: 1, 2 or 3 s for the blue and white LEDs and 15, 30, 60 and 300 s for the blue and white EL. For comparison between the different types of illumination, we used two measures: the signal/noise (S/N) values at 5 nM of the unquenched SNAP-25 peptide and the limit of detection (LOD) of the peptide. Examples of the actual CCD images using the various types of excitation are shown in Figure 3 with the corresponding ImageJ 3D graph analysis of CCD images showing the pixel intensity. The signal from the blue EL excitation exposure of 60 s is low (Figure 3, CCD image

NIH-PA Author Manuscript

NIH-PA Author Manuscript

NIH-PA Author Manuscript

I). Increasing the exposure time to 300 s improves the signal (Figure 3, CCD image II), however, there appears to be an increase in the pixel-to-pixel signal variability within each well spot (the well spots looks “rough”), especially when compared with the blue LED excitation exposure of 2 s (Figure 3, CCD image III), which produced uniform “smooth” looking spot intensities within a well. The detailed 3D analysis (Figure 3, Graph II) shows the variability of the EL excitation clearly. While the shapes in the 3D graph of the blue LED spots are smooth cones (Figure 3, Graph III), the blue EL spots have an irregular rough surface (Figure 3, Graph II) representing pixel-pixel variations. The variation of light intensity for the EL illumination strips is also shown in Figures 2C and 2D, where the EL lines of the spectra are noisy, demonstrating variation in intensity. Figure 3 IV (CCD image and Graph) show the corresponding data for the white LED a 3 s exposure, clearly the background appears somewhat higher than the blue LED in this case. In general, the longer the exposure time the higher the standard deviation (SD) of the measurements. Because we average the value of all the pixels within a well spot, such variation may not have significance, except at low signal where a high background may mask the signal, the increase in the pixel-to-pixel signal variability is critical for analyzing small elements (e.g. microarray spots).

The signal intensities from these CCD images of the unquenched SNAP-25 were measured using ImageJ and then analyzed in Microsoft Excel. The dose response curves for each of the excitation sources are plotted in Figure 4. The results of these experiments appear to fall into three groups based on S/N and the SD at 5 nM. The first group with S/N of 16-30 (Figures 4A for the whole range of SNAP-25 and 4B for the low concentrations of SNAP-25), includes all the exposure times with the blue LED (1, 2 and 3 s) and the 5 min blue EL illumination. Within the group, the signals clustered in a narrow range in which the signals are not well separated. These illumination conditions provide the base S/N values. The second group, with S/N of 4-8 (Figures 4C for the whole range of SNAP-25 and 4D for the low concentrations of SNAP-25), is comprised of white LED exposure (1, 2 and 3 s) and the shorter blue EL exposures (15, 30, and 60 s). These illuminations are useful for the high concentrations (figure 4C) but not the low concentrations (figure 4D). A third group with S/N of ~3 (Figures 4E and 4F) includes the white EL exposures (15, 30, and 60 s), all with very high SDs (Figure 4F), so these illumination conditions are not useful. The white EL produces low intensity illumination spread over a wide spectrum, including the green range, which increases the background. Due to its high background the white EL was not used further in this study. The remainder of the study investigated the blue LED, white LED, and the blue EL as illumination/excitation sources.

3.4 LED-CCD and EL-CCD Detector Based Detection of LcA Activity

For the botulinum toxin activity FRET assay, the SNAP-25 peptide substrate of BoNT-A is labeled with the FITC donor/DABCYL acceptor FRET pair. The close proximity of the DABCYL causes significant quenching of FITC fluorescence. Interaction of the substrate with the toxin light chain LcA (or the full toxin BoNT-A) results in cleavage of the peptide sequence, disrupting the FRET and resulting in a concomitant increase in FITC fluorescence at 523 nm measured by CCD (see Supporting Information Figure S1). For the FRET cleavage assay, unlike the optimization analysis using unquenched FITC-labeled peptide (described in Section 3.3), the quenched peptide FITC/DABCYL-SNAP-25 was used at a fixed 5 μM concentration and exposed to different concentrations of a 2-fold LcA serial dilution in the range 0.078 nM – 20 nM, with a zero blank included as a control.

As with the optimization studies, three 30-well chips (A, B and C) were used with three replicas of each concentration of LcA in each chip. The assay was incubated for 2 hours in reactions tubes at 37 degrees C before being transferred to the assay chips and the cleaved SNAP-25 FITC fluorescence measured. To evaluate the LED-CCD detection capabilities for the LcA cleavage activity assay, based on the results of the optimization studies (Figure 4), we used

NIH-PA Author Manuscript

NIH-PA Author Manuscript

NIH-PA Author Manuscript

only the white and the blue LEDs plus the blue EL for excitation. Various exposure times for each illumination mode were used, ranging from 2-3 s for the blue and white LED and 30-300 s for the blue EL. The signal intensities from the CCD images were measured using ImageJ and then analyzed in Microsoft Excel. From these image intensities, dose response curves were plotted for each of the chips, see Figure 5, and limits of detection (LOD) determined. The LOD represents a measured concentration that generates a signal 3 standard deviations above background (no LcA), the limits of quantitation (LOQ) which is the limit at which the method can measure the difference between two different values, is about 1 nM (Figures 5B and 5C). The analysis of the three chips, with each chip containing three replicas of the LcA (nM) concentration range studied, are summarized in Table 1.

While there is a fairly strong agreement in the LOD values between chip B and chip C, the LOD values of chip A were significantly higher. Similarly, the results from chip A were also higher than our previously published value (1.25 nM LcA) of the same assay excited by the same EL used in our previous detector platform design [47], suggesting that the cleavage assay in chip A did not work well. Based on this, the data from chip A were not used further for the analysis.

The S/N ratio of the three replicas (e.g. measurement of the same LcA concentration excited with the same illumination) of each measurement was analyzed on chip B and chip C (Figure 5A). The data suggest a high correlation ($r^2 = 0.9952$) between the corresponding measurements in chip B and chip C. The plots of the data of chip B (Figure 5B) and of chip C (Figure 5C) show that the S/N ratio increases with the increasing LcA concentration for all methods of excitation.

The results in Table 1 show that the LOD for the assay using blue LED (for both 2 and 3 s) was similar to that for assays using illumination with the blue EL in 60 s and 300 s (5 min) exposures (0.078 nM LcA). The LOD using white LED (for both 2 and 3 s) was higher (1.40625 nM LcA). These data suggest that the LOD for the detector is in the range of 0.078 nM-1.41 nM LcA, depending on the illumination source and the exposure time. The average noise values (Arbitrary Units - AU) of the white LED are high (21337 AU), with a high SD (average 1809 AU) compared to the low noise of the blue LED (average 7810 AU), which also has a lower SD (average 234 AU), determined from blank (no LcA) wells. The high noise observed with white LED excitation may explain the lower sensitivity obtained. As discussed above, the white LED emits green light which, although, should be mostly blocked by the excitation/emission filter combination, still appears to give a much higher background signal than the blue LED (Figure 2A and 2B), and thus increases the level of noise.

The LOQ measured here is similar to the LOD reported in our previous work (1.25 nM LcA) [47] which was comparable to limit of detection (1 nM) of a similar assay [49] with SNAP-25 peptide substrate labeled with a different FRET pair and measured the output with a standard fluorimeter. However, the current combination of LED illumination and CCD detection (LED-CCD) was able to measure concentrations lower, down to 0.078 nM LcA (~10 ng/ml). The increased sensitivity is enhanced by the use of a different camera and higher intensity illumination.

The LOD of various immunoassay formats including ELISAs [4], commercial lateral flow test kits [7] and fluorescent immunoassays [50] is in the ng/ml range (2-50 ng/ml). More sophisticated detection schemes, such as those combining paramagnetic beads and electrochemiluminescent immunoassays, have measured down to 50 pg/ml of BoNT-A [10], however, such assays measure toxin presence and not activity. The most sensitive cleavage assay was reported to detect as little as 10 pg/ml [34,35] (similar to the sensitivity of the mouse bioassay) by first concentrating the toxin with immunomagnetic beads coupled to monoclonal

NIH-PA Author Manuscript

NIH-PA Author Manuscript

NIH-PA Author Manuscript

antibodies directed against the 100-kDa heavy chain subunit. This immunoseparation step could be added to our protocol to increase its sensitivity, although it would slow the overall assay time. While the main advantage of the EL illuminator is that it is simple and very inexpensive to fabricate, the blue LED allows the use of a broader range of wavelength (LEDs are available in numerous wavelengths). The higher light intensity of LEDs enables significantly shorter exposure times, no longer than two seconds, in contrast to the EL illumination which required a minimum of 60 seconds to achieve a similar LOD.

4. Conclusion

Applications that involve the detection and typing of BoNT may require a portable (e.g. in the field without a laboratory) and rapid detection system that is simple to use. The modular design BoNT-A detector described here enabled activity detection of BoNT-A. Using LED-based illumination as opposed to EL strips significantly reduced the exposure time required to measure the assay chip.

The multi-wavelength spatial LED illumination, enable excitation in a broad spectrum and the detection of many fluorophores make this system a versatile optical detector for many fluorescence detection applications, and enable the end user simple switching of excitation wavelengths (using a switch) when studying different fluorescent systems. In general, LED illumination is more uniform and intense than the EL illumination.

The best illumination conditions with S/N of 16-30 (Figures 4A for the whole range of SNAP-25 and 4B for the low concentrations of SNAP-25) are the exposure with the blue LED (1, 2 and 3 s) and the 5 min blue EL illumination. The main advantage of the LED with EL is the short exposure time (several seconds vs. several minutes). The use of the wide spectrum white LED offers a different advantage by allowing the use of a large number of fluorophores. However, the white LED generates a higher level of noise, which reduces sensitivity, so it requires the use of a filter with very narrow bands. The white EL produces very poor results both in terms of noise and exposure time so it is not useful for fluorescence detection.

The prototype LED-CCD detector platform presented here is portable, with all modular components enclosed in a small plastic container, and controlled using a laptop computer via a USB connection. The relative simplicity, ease of use, and physical properties of these LEDs illumination platforms makes them ideal candidates as an excitation source for a number of applications including lab-on-a-chip and for point-of care detection, especially for underserved populations, and many other applications that require on-site measurements.

Supplementary Material

Refer to Web version on PubMed Central for supplementary material.

Acknowledgments

This work was supported in part by the Office of Public Health emergency Preparedness (OPHEP) IAG 224-05-655 (to A. Rasooly) and by FDA contract HHSF223200610765P (to Dr. Yordan Kostov).

Biographies

Steven Sun studied at the University of Maryland Baltimore County (UMBC) and received a BS in computer engineering in 2007. He continued his education at UMBC and is currently pursuing a MS in computer engineering with a focus in optics and chip design, and biosensors. In 2007 he began work as a research engineer at the US Food and Drug Administration (FDA) in the Office of Science and Engineering Laboratories (OSEL). His work involves

NIH-PA Author Manuscript

NIH-PA Author Manuscript

NIH-PA Author Manuscript

biotechnology and applications of computer engineering in the biosensor field for public health safety.

Jesse Francis earned a BS in Biological Sciences from the University of Baltimore County (UMBC) in 2009. He worked as a lab assistant at US Food and Drug Administration (FDA) in the Office of Science and Engineering Laboratories (OSEL) from 2007 to 2008. He is currently a Research Specialist at ABL Inc. in Kensington, MD.

Kim E. Sapsford studied chemistry at the University of East Anglia (UEA, Norwich, UK) and in 2001 received her PhD in analytical chemistry developing optical biosensors. In 2001 she moved to the Center for Bio/Molecular Science and Engineering at the US Naval Research Laboratory, where she worked (until 2007) on creating fluorescent-based biosensors using the Array Biosensor technology developed by Dr. Frances Ligler. Currently she is a Staff Fellow at the US Food and Drug Administration (FDA) in the Office of Science and Engineering Laboratories (OSEL), Division of Biology (DB). Her work involves assessing biotechnology concerning public health safety in particular future biosensing technologies.

Yordan Kostov received his B.Sc. and M.Sc. with honors in 1987 from Department of Electrical Engineering, Odessa Politechnic Institute, Former USSR. He received a Ph.D. Degree in Electrical/Chemical Engineering from Bulgarian Academy of Sciences. From 1994 to 1999 he was an Assistant Professor in the Department of Biotechincs, Sofia Technical University, Bulgaria. After post-doctoral fellowship at Medical Biotechnology Center,University of Maryland Biotechnology Institute, in 2000 he became Research Assistant Professor at the Department of Chemical and Biochemical Engineering, University of Maryland, Baltimore County (UMBC). Since 2006 he is a Research Associate Professor at the same department, and he also holds a position as an Assistant Director of the Center for Advanced Sensor technology at the same University. He is involved in the development of chemical and biochemical sensor systems for biotechnology and biomedical applications.

Avraham Rasooly obtained a BSc in Agronomy from the Hebrew University Faculty of Agriculture in 1978, an MSc in Genetics from the Hebrew University Department of Genetics, in 1982 and a PhD from the Michigan State University Dept. of Crop & Soil Science in 1988 for research on microbial nitrogen fixation. From 1988 to 1990, he conducted postdoctoral research first at Michigan State University on the genetics of fungal lignin degradation, and then from 1990 to 1995 as a Research Assistant Professor/Senior Research Scientist in the Dept. of Molecular Pathogenesis, Skirball Institute NYU Medical Center and the Public Health Research Institute of New York working on microbial genetics, the regulation of plasmid replication and *S. aureus* pathogenesis. Dr. Rasooly joined the Food and Drug Administration (FDA) as a Microbiologist in 1995, where he is developing microbial detection approaches for foodborne pathogens and their toxins using biosensors and DNA microarrays. Currently Dr. Rasooly holds a joint FDA Center for Devices and Radiological Health (CDRH) and National Cancer Institute (NCI) appointment, continuing his research on microbial detection at FDA and serving as a program director at the Cancer Diagnostics Program of NCI, where he oversees research on novel technologies of cancer diagnostics.

References

1. Peruski AH, Johnson LH 3rd, Peruski LF Jr. Rapid and sensitive detection of biological warfare agents using time-resolved fluorescence assays. J Immunol Methods 2002;263:35–41. [PubMed: 12009202]
2. Sharma SK, Ferreira JL, Eblen BS, Whiting RC. Detection of type A, B, E, and F Clostridium botulinum neurotoxins in foods by using an amplified enzyme-linked immunosorbent assay with digoxigenin-labeled antibodies. Appl Environ Microbiol 2006;72:1231–8. [PubMed: 16461671]

NIH-PA Author Manuscript

NIH-PA Author Manuscript

NIH-PA Author Manuscript

3. Keller JE, Nowakowski JL, Filbert MG, Adler M. Rapid microplate assay for monitoring botulinum neurotoxin B catalytic activity. J Appl Toxicol 1999;19(Suppl 1):S13–7. [PubMed: 10594893]
4. Han SM, Cho JH, Cho IH, et al. Plastic enzyme-linked immunosorbent assays (ELISA)-on-a-chip biosensor for botulinum neurotoxin A. Anal Chim Acta 2007;587:1–8. [PubMed: 17386746]
5. Guglielmo-Viret V, Attree O, Blanco-Gros V, Thullier P. Comparison of electrochemiluminescence assay and ELISA for the detection of Clostridium botulinum type B neurotoxin. Journal of immunological methods 2005;301:164–72. [PubMed: 15979637]
6. Ferreira JL, Eliasberg SJ, Edmonds P, Harrison MA. Comparison of the mouse bioassay and enzyme-linked immunosorbent assay procedures for the detection of type A botulinal toxin in food. J Food Prot 2004;67:203–6. [PubMed: 14717376]
7. Gessler F, Pagel-Wieder S, Avondet MA, Bohnel H. Evaluation of lateral flow assays for the detection of botulinum neurotoxin type A and their application in laboratory diagnosis of botulism. Diagn Microbiol Infect Dis 2007;57:243–9. [PubMed: 17141460]
8. Sharma SK, Eblen BS, Bull RL, Burr DH, Whiting RC. Evaluation of lateral-flow Clostridium botulinum neurotoxin detection kits for food analysis. Applied and environmental microbiology 2005;71:3935–41. [PubMed: 16000807]
9. Gessler F, Hampe K, Schmidt M, Bohnel H. Immunomagnetic beads assay for the detection of botulinum neurotoxin types C and D. Diagn Microbiol Infect Dis 2006;56:225–32. [PubMed: 16839735]
10. Rivera VR, Gamez FJ, Keener WK, White JA, Poli MA. Rapid detection of Clostridium botulinum toxins A, B, E, and F in clinical samples, selected food matrices, and buffer using paramagnetic bead-based electrochemiluminescence detection. Analytical biochemistry 2006;353:248–56. [PubMed: 16620745]
11. Gessler F, Hampe K, Bohnel H. Sensitive detection of botulinum neurotoxin types C and D with an immunoaffinity chromatographic column test. Applied and environmental microbiology 2005;71:7897–903. [PubMed: 16332765]
12. Attree O, Guglielmo-Viret V, Gros V, Thullier P. Development and comparison of two immunoassay formats for rapid detection of botulinum neurotoxin type A. Journal of immunological methods 2007;325:78–87. [PubMed: 17659299]
13. Golden J, Shriver-Lake L, Sapsford K, Ligler F. A “do-it-yourself” array biosensor. Methods 2005;37:65–72. [PubMed: 16202623]
14. Ligler FS, Sapsford KE, Golden JP, et al. The array biosensor: portable, automated systems. Anal Sci 2007;23:5–10. [PubMed: 17213615]
15. Ligler FS, Taitt CR, Shriver-Lake LC, Sapsford KE, Shubin Y, Golden JP. Array biosensor for detection of toxins. Analytical and bioanalytical chemistry 2003;377:469–77. [PubMed: 12811462]
16. Phillips RW, Abbott D. High-throughput enzyme-linked immunoabsorbant assay (ELISA) electrochemiluminescent detection of botulinum toxins in foods for food safety and defence purposes. Food additives & contaminants 2008;25:1084–8.
17. Ganapathy R, Padmanabhan S, Eric YP, Moochhala S, Lionel LK, Ponnampalam G. Rapid detection of botulinum neurotoxins A, B, E, and F by optical immunoassay. Front Biosci 2008;13:5432–40. [PubMed: 18508597]
18. Volland H, Lamourette P, Nevers MC, et al. A sensitive sandwich enzyme immunoassay for free or complexed Clostridium botulinum neurotoxin type A. J Immunol Methods 2008;330:120–9. [PubMed: 18093612]
19. Chiao DJ, Wey JJ, Shyu RH, Tang SS. Monoclonal antibody-based lateral flow assay for detection of botulinum neurotoxin type A. Hybridoma (2005) 2008;27:31–5. [PubMed: 18294074]
20. CDC. Botulism in the United States 1899-1996: Handbook for Epidemiologists, Clinicians, and Laboratory Workers. Centers for Disease Control and Prevention; Atlanta, Ga: 1998.
21. Nowakowski A, Wang C, Powers DB, et al. Potent neutralization of botulinum neurotoxin by recombinant oligoclonal antibody. Proc Natl Acad Sci U S A 2002;99:11346–50. [PubMed: 12177434]
22. Keller JE. Recovery from botulinum neurotoxin poisoning in vivo. Neuroscience. 2006
23. Schantz EJ, Johnson EA. Dose standardisation of botulinum toxin. Lancet 1990;335:421. [PubMed: 1968156]

NIH-PA Author Manuscript

NIH-PA Author Manuscript

NIH-PA Author Manuscript

24. Schantz EJ, Johnson EA. Properties and use of botulinum toxin and other microbial neurotoxins in medicine. Microbiol Rev 1992;56:80–99. [PubMed: 1579114]
25. Shone CC, Quinn CP, Wait R, Hallis B, Fooks SG, Hambleton P. Proteolytic cleavage of synthetic fragments of vesicle-associated membrane protein, isoform-2 by botulinum type B neurotoxin. Eur J Biochem 1993;217:965–71. [PubMed: 8223654]
26. Schiavo G, Benfenati F, Poulain B, et al. Tetanus and botulinum-B neurotoxins block neurotransmitter release by proteolytic cleavage of synaptobrevin. Nature 1992;359:832–5. [PubMed: 1331807]
27. Schiavo G, Poulain B, Rossetto O, Benfenati F, Tauc L, Montecucco C. Tetanus toxin is a zinc protein and its inhibition of neurotransmitter release and protease activity depend on zinc. Embo J 1992;11:3577–83. [PubMed: 1396558]
28. Sudhof TC, De Camilli P, Niemann H, Jahn R. Membrane fusion machinery: insights from synaptic proteins. Cell 1993;75:1–4. [PubMed: 8402889]
29. Blasi J, Chapman ER, Link E, et al. Botulinum neurotoxin A selectively cleaves the synaptic protein SNAP-25. Nature 1993;365:160–3. [PubMed: 8103915]
30. Schiavo G, Rossetto O, Catsicas S, et al. Identification of the nerve terminal targets of botulinum neurotoxin serotypes A, D, and E. J Biol Chem 1993;268:23784–7. [PubMed: 8226912]
31. Trimble WS. Analysis of the structure and expression of the VAMP family of synaptic vesicle proteins. J Physiol Paris 1993;87:107–15. [PubMed: 8305898]
32. Dong M, Tepp WH, Johnson EA, Chapman ER. Using fluorescent sensors to detect botulinum neurotoxin activity in vitro and in living cells. Proc Natl Acad Sci U S A 2004;101:14701–6. [PubMed: 15465919]
33. Kalb SR, Moura H, Boyer AE, McWilliams LG, Pirkle JL, Barr JR. The use of Endopep-MS for the detection of botulinum toxins A, B, E, and F in serum and stool samples. Analytical biochemistry 2006;351:84–92. [PubMed: 16500606]
34. Rasooly R, Stanker LH, Carter JM, et al. Detection of botulinum neurotoxin-A activity in food by peptide cleavage assay. International journal of food microbiology 2008;126:135–9. [PubMed: 18571757]
35. Rasooly R, Do PM. Development of an in vitro activity assay as an alternative to the mouse bioassay for Clostridium botulinum neurotoxin type A. Appl Environ Microbiol 2008;74:4309–13. [PubMed: 18515481]
36. Jones RG, Liu Y, Sesardic D. New highly specific botulinum type C1 endopeptidase immunoassays utilising SNAP25 or Syntaxin substrates. J Immunol Methods. 2009
37. Kegel B, Behrensdorf-Nicol HA, Bonifas U, et al. An in vitro assay for detection of tetanus neurotoxin activity: using antibodies for recognizing the proteolytically generated cleavage product. Toxicol In Vitro 2007;21:1641–9. [PubMed: 17826026]
38. Jones RG, Ochiai M, Liu Y, Ekong T, Sesardic D. Development of improved SNAP25 endopeptidase immuno-assays for botulinum type A and E toxins. J Immunol Methods 2008;329:92–101. [PubMed: 17976638]
39. Boldt GE, Kennedy JP, Hixon MS, et al. Synthesis, characterization and development of a high-throughput methodology for the discovery of botulinum neurotoxin a inhibitors. Journal of combinatorial chemistry 2006;8:513–21. [PubMed: 16827563]
40. Perpetuo EA, Juliano L, Juliano MA, et al. Enzymatic profiling of tetanus and botulinum neurotoxins based on vesicle-associated-membrane protein derived fluorogenic substrates. Protein and peptide letters 2008;15:1100–6. [PubMed: 19075822]
41. Pires-Alves M, Ho M, Aberle KK, Janda KD, Wilson BA. Tandem fluorescent proteins as enhanced FRET-based substrates for botulinum neurotoxin activity. Toxicon 2009;53:392–9. [PubMed: 19168088]
42. Hines HB, Kim AD, Stafford RG, et al. Use of a recombinant fluorescent substrate with cleavage sites for all botulinum neurotoxins in high-throughput screening of natural product extracts for inhibitors of serotypes A, B, and E. Appl Environ Microbiol 2008;74:653–9. [PubMed: 18083881]
43. Bagramyan K, Barash JR, Arnon SS, Kalkum M. Attomolar detection of botulinum toxin type A in complex biological matrices. PLoS ONE 2008;3:e2041. [PubMed: 18446228]
44. Frisk ML, Berthier E, Tepp WH, Johnson EA, Beebe DJ. Bead-based microfluidic toxin sensor integrating evaporative signal amplification. Lab Chip 2008;8:1793–800. [PubMed: 18941677]

NIH-PA Author Manuscript

NIH-PA Author Manuscript

NIH-PA Author Manuscript

45. Mangru S, Bentz BL, Davis TJ, et al. Integrated Bioassays in Microfluidic Devices: Botulinum Toxin Assays. J Biomol Screen 2005;10:788–94. [PubMed: 16234350]

46. Sapsford KE, Sun S, Francis J, Sharma S, Kostov Y, Rasooly A. A fluorescence detection platform using spatial electroluminescent excitation for measuring botulinum neurotoxin A activity. Biosens Bioelectron 2008;24:618–25. [PubMed: 18644709]

47. Sapsford KE, Sun S, Francis J, Sharma S, Kostov Y, Rasooly A. A fluorescence detection platform using spatial electroluminescent excitation for measuring botulinum neurotoxin A activity. Biosensors & bioelectronics. 2008

48. Sapsford KE, Francis J, Sun S, Kostov Y, Rasooly A. Miniaturized 96-well ELISA chips for staphylococcal enterotoxin B detection using portable colorimetric detector. Analytical and bioanalytical chemistry. 2009

49. Schmidt JJ, Stafford RG. Fluorigenic substrates for the protease activities of botulinum neurotoxins, serotypes A, B, and F. Applied and environmental microbiology 2003;69:297–303. [PubMed: 12514008]

50. Sapsford KE, Taitt CR, Loo N, Ligler FS. Biosensor detection of botulinum toxoid A and staphylococcal enterotoxin B in food. Applied and environmental microbiology 2005;71:5590–2. [PubMed: 16151154]

NIH-PA Author Manuscript
NIH-PA Author Manuscript
NIH-PA Author Manuscript

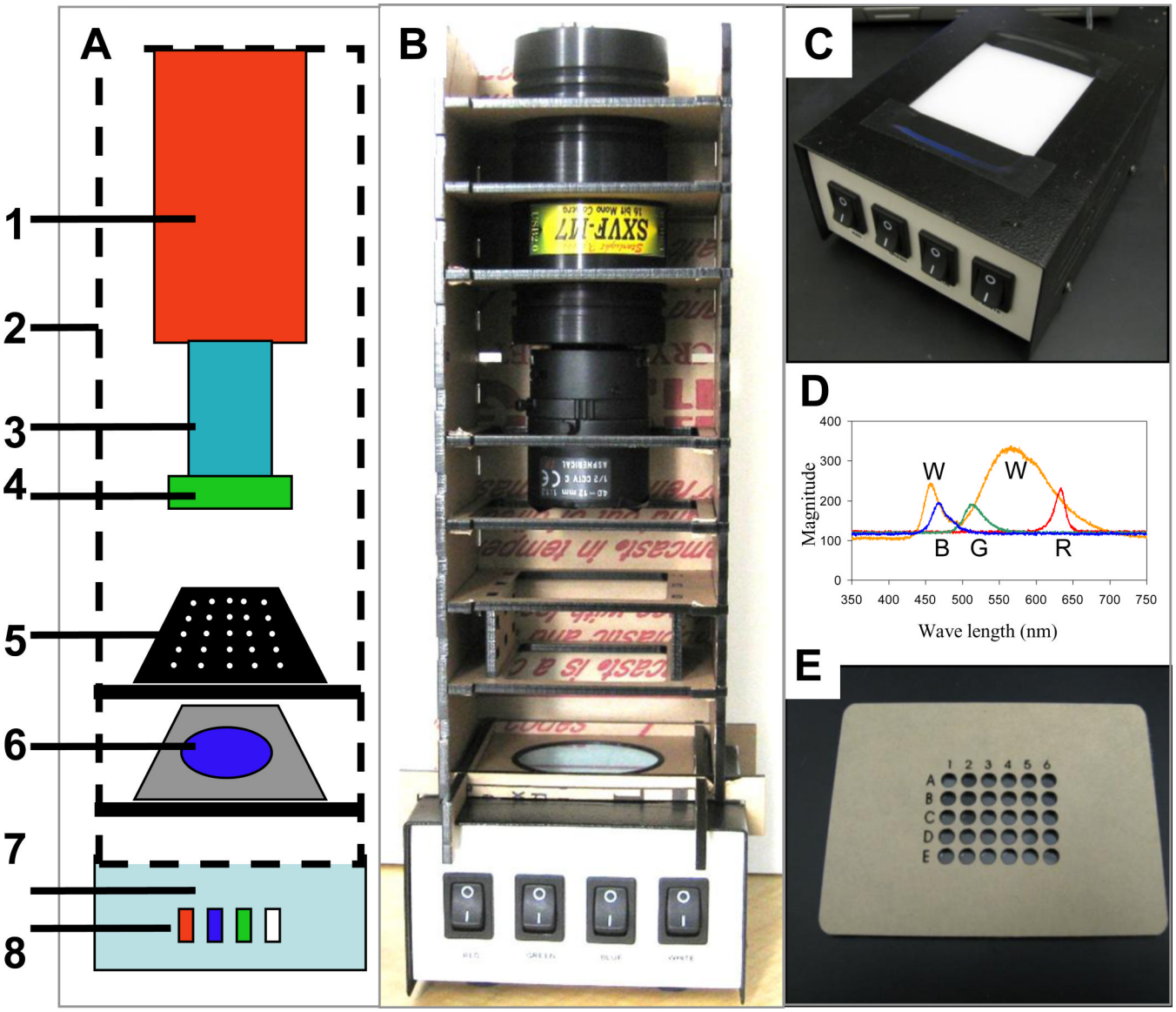

Figure 1. LED-CCD multi-wavelength detector

(A) A schematic configuration of the multi-wavelength LED detector. **(B)** A digital camera image of the actual detector platform. The detector system components highlighted in the schematic (A) are [1] an SXVF-M7 CCD camera mounted in a homemade acrylic shelf box [2], which was designed to hold the filters and the sample chips. The camera is equipped with a Tamron manual zoom CCTV 4-12 mm, f1.2 C-mount lens [3] with a green band pass emission filter [4] mounted on the end of the lens. The black acrylic 30-well sample chip [5] (also panel E) is placed on a shelf in the camera box above the blue band pass excitation filter [6]. The camera shelf box is placed on the top of the multi-wavelength LED illuminator [7] (also panel C) with light switches to operate the red, blue, green and white LEDs [8]. **(C)** Digital photograph of the multi-wavelength LED illuminator prior to attachment of the shelf box. **(D)** Spectra of the white (W), blue (B), green (G) and red (R) LEDs that comprise the multi-wavelength LED illuminator. **(E)** The black acrylic 30-well chips designed to hold aqueous samples for imaging.

NIH-PA Author Manuscript

NIH-PA Author Manuscript

NIH-PA Author Manuscript

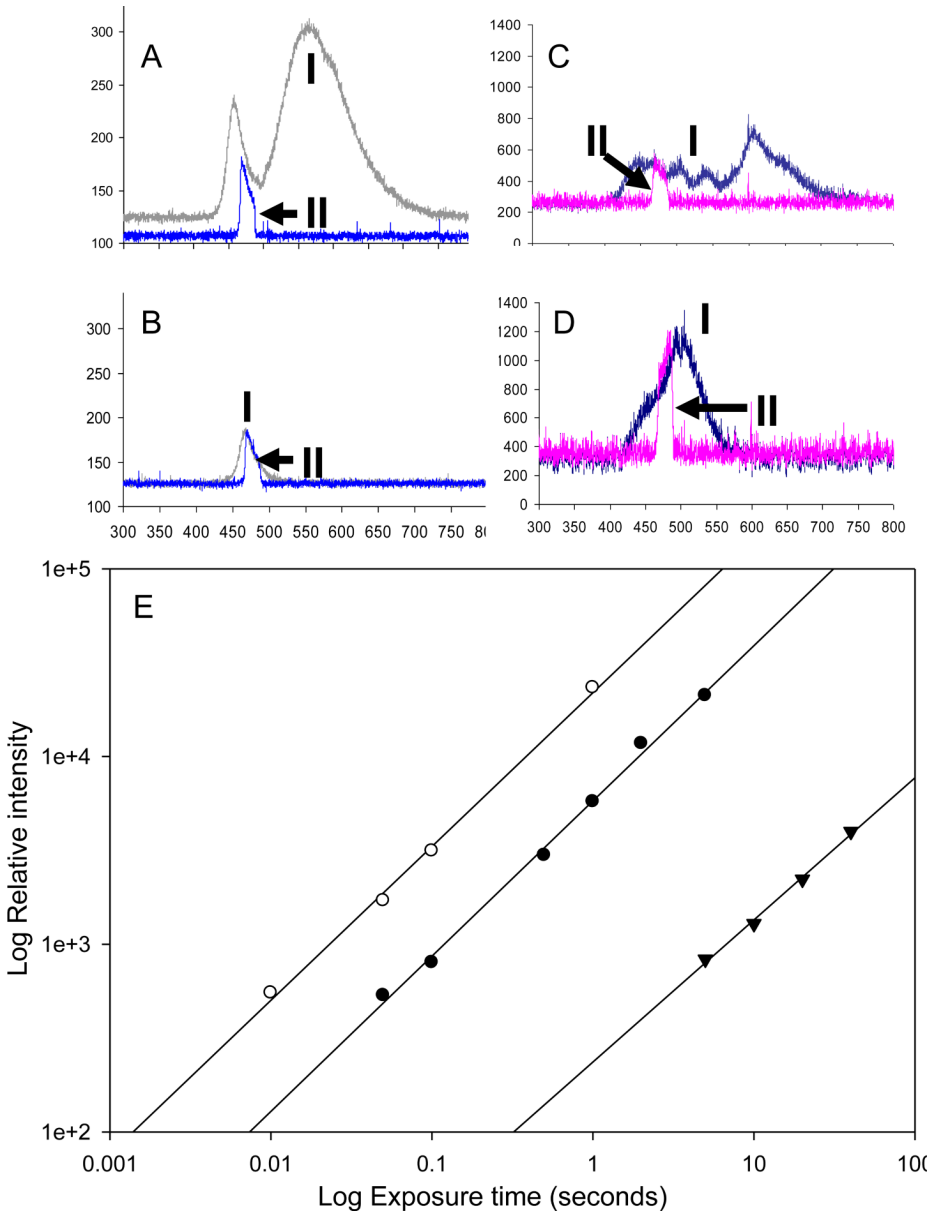

Figure 2. Light characteristics of the EL and LED illumination sources

The spectra (measured by a spectrometer) and the light intensity of the LED were measured for the **(A)** white LED and the **(B)** blue LED illuminators (exposure time 100 ms) compared with the **(C)** white EL and **(D)** blue EL strips (exposure time 5 s). In panels A-D, the upper plots are measurements of the whole spectra (I) and the lower plots (II marked with arrows) are spectra measured with the blue filter, used for excitation of the FITC dye, in place. To evaluate the actual signal from the assay, the fluorescence signal of 5 nM unquenched SNAP-25 peptide (labeled with FITC) was measured with various exposure times (ranging from 10 ms to 10 s) using a cooled CCD camera equipped with a blue emission filter and a green excitation filter. **(E)** The signal intensity measured at the CCD plotted as a function of exposure time for the different excitation sources white LED (white circles), blue LED (black circles), and the blue EL panel (black triangles). Note that both the exposure time axis and the relative intensity axis are plotted on a log scale.

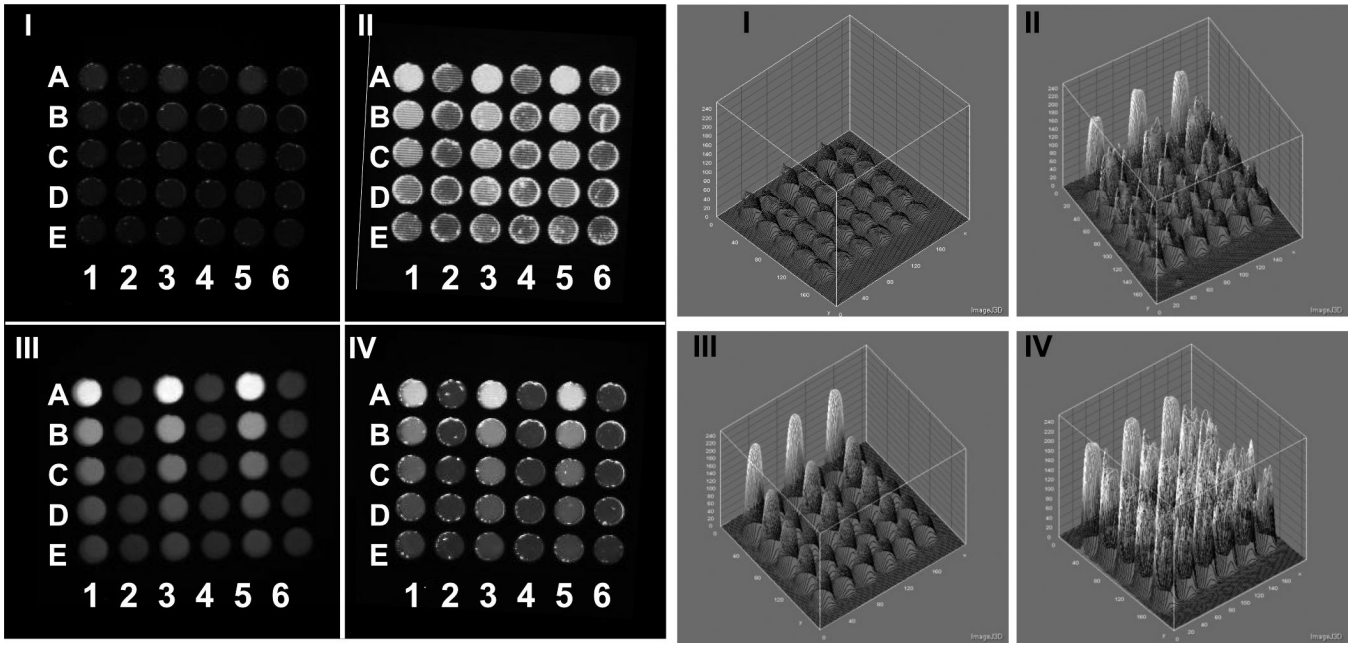

Figure 3. CCD Images and 3D analysis of EL-CCD and LED-CCD detection of unquenched FITC-SNAP peptide

The CCD images and the corresponding 3D imageJ analysis of the CCD emission images of nine concentrations of a 50% dilution series of the unquenched SNAP-25 peptide ranging from 0.019 nM to 5 nM and a control are shown for: (I) blue EL excitation exposure of 60 seconds, (II) blue EL excitation exposure of 300 s, (III) blue LED excitation exposure of 2 s and (IV) white LED excitation exposure of 3 s.

NIH-PA Author Manuscript
NIH-PA Author Manuscript
NIH-PA Author Manuscript

NIH-PA Author Manuscript

NIH-PA Author Manuscript

NIH-PA Author Manuscript

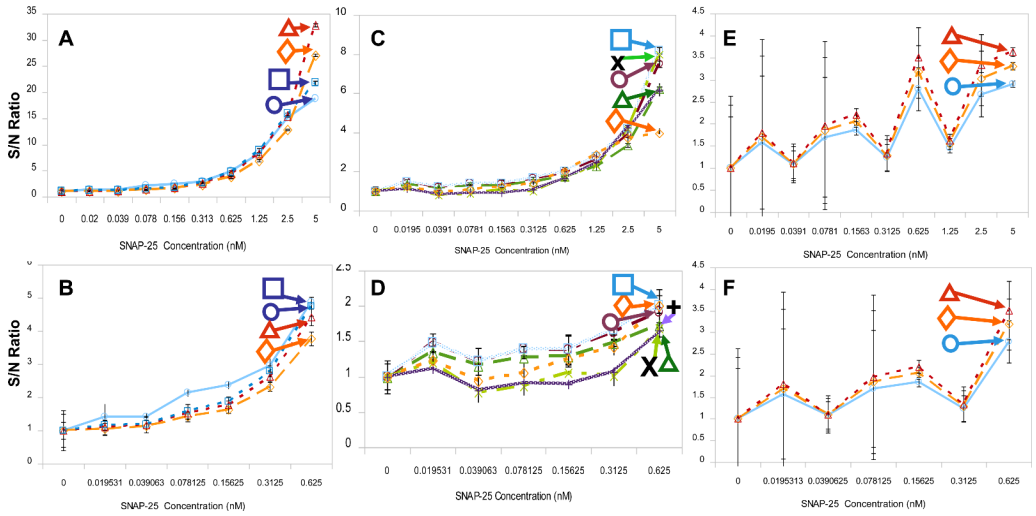

Figure 4. LED-CCD fluoresce analysis of unquenched SNAP-25 peptide

A 50% dilution series of the unquenched SNAP-25 (labeled with FITC) and a control (no SNAP-25) was prepared, giving 10 samples with a final concentration range of 0 nM-5 nM. The dilution series was loaded in triplicate into each 30-well chip and the fluorescence excited using either the LED or EL illuminators. The CCD camera was used for detection. The signal-to-noise (S/N) ratio for CCD measured intensity as a function of the SNAP concentration was plotted for each of the EL and LED excitation method used. **(A)** Blue LED illumination (1 s-diamond, 2 s-triangle and 3 s-rectangle) and blue EL illumination (5 min-circle). **(B)** Expansion of the lower concentration range, 0 nM-0.625 nM, of SNAP-25 dose response curve from (A). **(C)** White LED illumination (1 s-X, 2 s-vertical line and 3 s-diamond/dashed line) and the shorter exposure times used for the blue EL (15 s- triangle, 30 s,- circle and 60 s- rectangle). **(D)** Expansion of the lower concentration range for the SNAP-25 dose response plotted in (C). **(E)** White EL illumination (15 s- circle, 30 s-diamond and 60 s- triangle). **(F)** Expansion of the lower concentration range for the SNAP-25 dose response plotted in (E). Standard deviations were determined from three separate readings of each chip.

NIH-PA Author Manuscript

NIH-PA Author Manuscript

NIH-PA Author Manuscript

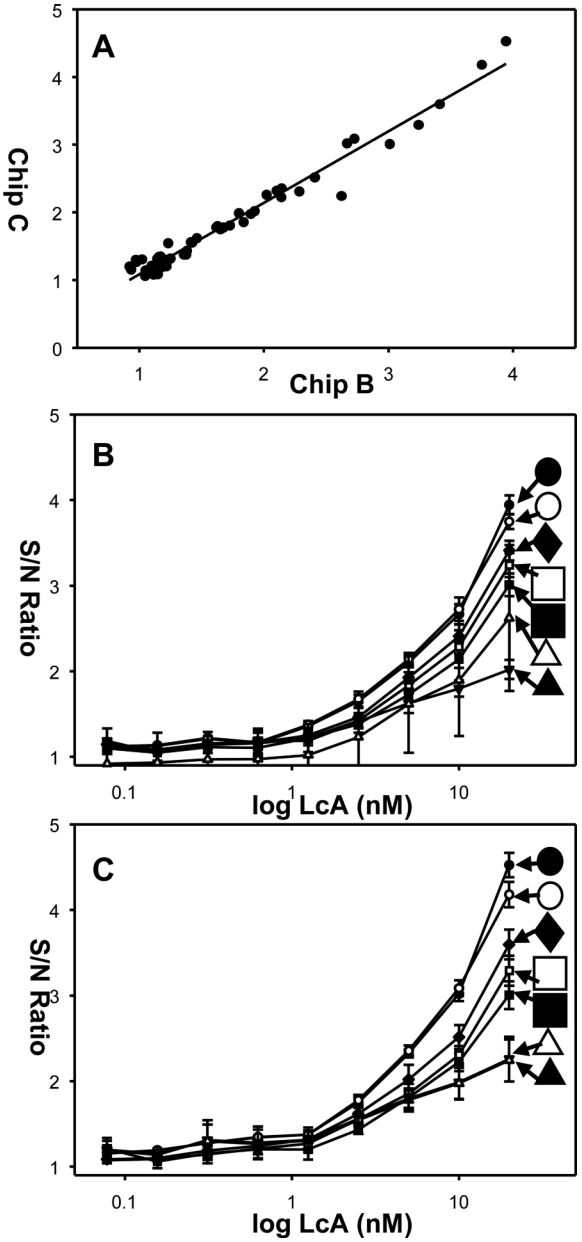

Figure 5. ***In vitro*** **activity analysis of BoNT-A light chain (LcA) cleavage of FITC/DABCYL-SNAP-25 peptide detected by FRET**

Various concentrations of LcA (0 nM-20 nM) were used to cleave FITC/DABCYL-SNAP-25 (5 μM). The cleavage products were excited by LED or EL and fluorescence intensity measured by CCD. **(A)** Correlation between the S/N ratio of the cleavage assay measurements in chip B and chip C. LcA dose response curves plotted as a function of the excitation source for **(B)** chip B and for (C) chip C. For both plots; blue LED exposure of 2 s (black circle), blue LED exposure of 3 s (white circle), white LED exposure of 3 s (black triangles), white LED exposure of 2 s (white rectangle), blue EL exposure of 30 s (black rectangle), blue EL exposure of 60 s (white rectangle), blue EL exposure of 300 s (black diamond). Note that the LcA concentration axis is plotted on the log scale, so the zero (blank) concentration is not present. Standard deviations were determined from three separate readings of each chip.

NIH-PA Author Manuscript
NIH-PA Author Manuscript
NIH-PA Author Manuscript

Table 1

Summary of LOD determined for LcA in nM, measured from 3 separate chips (A-C) using various excitation sources and different exposure times: Blue LED with 2 seconds exposure (B-LED 2s), Blue LED with 3 seconds exposure (B-LED 3s), White LED with 3 seconds exposure (W-LED 3s), White LED with 2 seconds exposure (W-LED 2s), Blue electroluminescent with 30 seconds exposure (B-EL 30s), Blue electroluminescent with 60 seconds exposure (B-EL 60s) and Blue electroluminescent with 5 minutes exposure (B-EL 5min)

Chip	B-LED 2s	B-LED 3s	W-LED 3s	W-LED 2s	B-EL 30s	B-EL 60s	B-EL 5min
A	**1.25**	**1.25**	**2.5**	**20**	**10**	**10**	**ND**
B	**0.078**	**0.156**	**0.312**	**0.312**	**1.25**	**0.078**	**0.078**
C	**0.078**	**0.078**	**2.5**	**2.5**	**0.078**	**0.0785**	**0.078**
Average*	0.078	0.117	1.406	1.406	0.664	0.078	0.078

Sens Actuators B Chem. Author manuscript; available in PMC 2011 April 8.